Catena 234 (2024) 107601

Contents lists available at ScienceDirect

Catena

journal homepage: www.elsevier.com/locate/catena

# Machine Learning-Based examination of recent mangrove forest changes in the western Irrawaddy River Delta, Southeast Asia

Yuan Xiong [a], Zhijun Dai [a,b,*], Chuqi Long [a], Xixing Liang [a], Yaying Lou [c], Xuefei Mei [a], Binh An Nguyen [d], Jinping Cheng [e]

[a] State Key Laboratory of Estuarine and Coastal Research, East China Normal University, Shanghai, China
[b] Laboratory for Marine Geology, Qingdao National Laboratory for Marine Science and Technology, Qingdao, China
[c] Zhuhai-M.U.S.T. Science and Technology Research Institute, Zhuhai, China
[d] Ho Chi Minh City Institute of Resources Geography, Vietnam Academy of Science and Technology, Ho Chi Minh City, Viet Nam
[e] Department of Science and Environmental Studies, The Education University of Hong Kong, New Territories, Hong Kong, China

ARTICLE INFO

*Keywords:*
Dynamics
Mangrove forest
Gain and loss
The western Irrawaddy River Delta
Anthropogenic activities
Southeast Asia

ABSTRACT

Mangrove forests serve as a significant carbon sink and provide effective shoreline protection against devastating winds. However, these forests are facing an unprecedented decline in tropical and subtropical large deltas due to human activities and climate change. This study focuses on quantifying the dynamic changes of mangrove forests in the Western Irrawaddy River Delta (WIDR), which is part of Myanmar's largest delta in Southeast Asia, Remote sensing images from 1988 to 2022 were utilized alongside a machine learning approach to analyze these changes. The findings demonstrate a significant decline of mangrove forests within the WIRD, with a reduction in area by 45.35% over the past 35 years. Additionally, the patches of mangrove forests have become increasingly fragmented. Losses predominantly occurred in the inland regions, while gains were observed along the seaward edges, suggesting progradation towards the sea, which compensated for a net loss of 2,812.32 ha during the study period. The intensification of human activities, specifically deforestation and aquaculture pond utilization, appears to be the leading cause of catastrophic internal degradation within the WIRD's mangrove forests. Contrary to the influence of local sea level rise or variations in suspended sediment discharge into the WIRD, this study suggests that the persistent retreat of mangrove forest fringes is controlled by large waves generated by the southwest monsoon. Estuarine barriers situated in the WIRD act as buffers, dissipating wave energy and facilitating seaward growth. of mangrove forests. Our study reveals a significant pattern in the WIRD, where landward mangrove forest loss coincided with seaward mangrove forest gain. This work underscores the importance of addressing landward mangrove forest loss and recognizing the emergence of seaward gains in the WIRD, providing valuable insights for fostering successful and sustainable mangrove management and protection initiatives.

## 1. Introduction

The mangrove forest is an essential coastal wetland ecosystem with high primary productivity in the tropical and subtropical intertidal zones (Clough, 1992). Globally mangrove forests cover nearly 147,000 $km^2$ of the coastal areas (Leal and Spalding, 2022), and serve as an essential global carbon sink (Duarte et al., 2013; Richards et al., 2020). Physically, mangrove forest serves as a protective barrier between marine and terrestrial ecosystems, providing biological resources and aiding in the preservation of biodiversity (Friess et al., 2019; Salem and Mercer, 2012). However, the global mangrove forests have experienced an unprecedented decline (Worthington et al., 2020), particularly in the latter half of the 20th century, with an annual area loss of 1% to 2% (Friess et al., 2019).

Despite a partial deceleration observed since the onset of the 21st century, the loss rate of mangrove forests continues to exhibit a substantial annual decline of approximately 0.4% (Hamilton and Casey, 2014). Notably, this rate surpasses the loss rates observed in neighboring coral reefs or tropical forests (Duke et al., 2007), underscoring the urgency of addressing the ongoing mangrove forest decline challenge. The

* Corresponding author at: State Key Laboratory of Estuarine and Coastal Research, East China Normal University, Shanghai, China.
*E-mail address:* zjdai@sklec.ecnu.edu.cn (Z. Dai).

https://doi.org/10.1016/j.catena.2023.107601
Received 24 May 2023; Received in revised form 13 October 2023; Accepted 14 October 2023

profound degradation of mangrove forests has significantly jeopardized the survival and socio-economic development of human communities (Carugati et al., 2018; Danielsen et al., 2005). Consequently, there is a global imperative to prioritize the protection, management, and sustainable development of mangrove ecosystems (Ellison et al., 2020).

Intertidal mangroves face a significant threat from sea-level rise within the context of global warming, as indicated by several research studies (Fanous et al., 2023; Krauss et al., 2014; Lovelock et al., 2015). An adequate upstream supply of suspended sediment originating from upstream sources plays a vital role in enhancing the resilience of mangrove forests against rising sea levels. Conversely, the insufficient delivery of sediment from major river systems heightens the susceptibility of mangrove ecosystems to submergence and subsequent loss (Kimeli et al., 2022; Long et al., 2021; Woodroffe et al., 2016).

Recent scientific investigations have emphasized hydrodynamics play a crucial role in shaping the distribution of mangrove forests. Low wave energy in estuaries promotes sediment resuspension, fostering favorable conditions for mangrove growth, while strong hydrodynamic forces drive the landward migration of mangrove forests (Long et al., 2022; Raw et al., 2022; Sánchez-Núñez et al., 2019; Xie et al., 2022). Furthermore, human activities have irreversible and detrimental impacts on mangrove forests (Leal and Spalding, 2022; Mokievsky et al., 2020). Illegal mangrove logging, expansion of aquaculture activities, and rapid urban development emerge as the primary drivers posing significant risks to the preservation of mangrove forests (Ai et al., 2020; Leal and Spalding, 2022; Tinh et al., 2022).

The urgent task of conserving and restoring mangrove resources necessitates the accurate mapping of the geographic distribution as well as monitoring the gains and losses of mangrove forests (Ellison et al., 2020; Jia et al., 2014; Zhang et al., 2023). Remote sensing stands out as one of the limited non-contact monitoring techniques capable of facilitating large-scale and synchronous measurements of delta mangroves, offering high temporal and spatial resolution (Giri, 2016). In recent years, there has been a surge in scientific studies utilizing remote sensing techniques combined with statistical analyses to examine the spatio-temporal dynamics of mangrove forest area changes across different countries (Conchedda et al., 2008; Ibharim et al., 2015; Liao et al., 2019; Murillo-Sandoval et al., 2022; Thu and Populus, 2007; Valderrama-Landeros et al., 2020), and regions (Guo et al., 2021; Mokievsky et al., 2020; Thomas et al., 2017; Valderrama-Landeros et al., 2020) and even across the globe (Bhowmik et al., 2022; Bunting et al., 2022; Giri et al., 2011; Jia et al., 2023), and these studies generated lots of mangrove atlas. The publicly available datasets have provided a preliminary understanding of the changes in mangrove forest extent, including losses, gains, and their associated drivers. However, these analyses primarily focus on bi-temporal or decadal assessments at large spatial scales. There is a notable lack of systematic data with high spatial and temporal resolution concerning mangrove forest gain and loss. Furthermore, limited information is available regarding the coastal dynamic forces influencing spatial changes in mangroves, particularly in the Western Irrawaddy River Delta (WIRD) in Myanmar, Southeast Asia. Despite being the third-largest mangrove forest area in Asia, WIRD lacks detailed information on its spatial changes. Therefore, it is crucial to employ long-term remote sensing imagery to generate accurate and up-to-date maps of the mangrove forests in the WIRD (Estoque et al., 2018; Spalding et al., 2010).

Landsat time-series images have been widely employed in the study of mangroves, proving to be the most suitable option for national or regional assessments (Gitau et al., 2023; Guo et al., 2021; Teluguntla et al., 2018). Among supervised machine learning methods, Random Forest (RF) has demonstrated superior effectiveness in identifying mangrove forests compared to other algorithms (Habibullah et al., 2023; Poortinga et al., 2020). In this study, Landsat time-series images were utilized in conjunction with the Random Forest model to investigate and map the status and dynamic change patterns of mangrove forests in the WIRD from 1988 to 2022. The objectives of this study were to: (1) quantify the extent of mangrove forests in the WIRD; (2) analyze the dynamic changes in mangrove forest shorelines; (3) assess mangrove gain-and-loss patterns and explore the potential driving factors behind the bio-morphodynamic changes in mangrove forests. This research contributes to understanding the bio-morphodynamics of mangrove forests under anthropogenic disturbance and climate change, providing valuable reference materials for the protection and sustainable management of mangrove resources worldwide.

## 2. Materials and methods

### 2.1. Study area

The western Irrawaddy River Delta, a part of one of the largest deltas in Southeast Asia (Fig. 1A), situated in southern Myanmar's central plain. It is Myanmar's lowest flat alluvial floodplain, which is also a typical tropical river delta (Giosan et al., 2017) governed by semi-diurnal tides with a 3–6 m tidal range (Brakenridge et al., 2017). The mangroves of the Irrawaddy River Delta are widespread and densely distributed in the western sector (Oo, 2002). Mangroves primarily flourish in the WIRD with coordinates of 94.22°E 95.78°E, 15.65°N 16.33°N, which spans an area of approximately 7,776.23 $km^2$ (Fig. 1B).

### 2.2. Materials

All available Landsat time-series remote sensing images (path 133 row 49) with a cloud cover of less than 50% from 1988 to 2022 were obtained from the Google Earth Engine (GEE) (https://earthengine.google.com) for mapping the interannual spatial distribution of mangrove forests. They include Landsat 5 TM (1988–2011), Landsat 7 ETM+ (2012–2013), Landsat 8 Operational Land Imager (OLI) (2013–2022), and Landsat 9 OLI-2 (2021–2022) from Collection 1 based on the World Geodetic System 1984 (WGS84) geographical coordinate system and Universal Transverse Mercator (UTM) projection coordinate system. Images are based on raw data using the National Aeronautics and Space Administration (NASA)'s Jet Propulsion Laboratory (JPL) developed single-channel algorithm for atmospheric correction. The pixels in the reflected signal that contain clouds, cirrus, cloud shadow, and air pollution were filtered out using the F-mask computed by the image quality assessment band, and then the annual median images were synthesized according to the resulting data. We counted the annual (Fig. 2) and mensal (Fig. S1) number of Landsat images from 1988 to 2022. We used a total of 520 images to generate mangrove forest maps after removing poor-quality observations, including clouds, shadows, and scan-line corrector (SLC) off gaps by quality assurance (QA) band.

The Shuttle Radar Topography Mission Digital Elevation Data (DEM) (Farr et al., 2000) was used to remove high-altitude locations with an elevation exceeding 40 m in the study area given the majority of mangrove forests are found in the lower altitude. Global Mangrove Watch Datasets (https://www.globalmangrovewatch.org/) and Google Earth historical images were used to create sample points for classification. Meanwhile, aiming to investigate the major driving factors of mangrove forests area change in the WIRD, we acquired 3 arc-second global DEM (GDEM) with higher spatial resolution(Zhang et al., 2022) and hydrological data, including suspended sediment discharge (SSD) between 1990 and 2010 in Magway station collected from (IFC, 2019), sea level rising from 1992 to 2022 obtained from NASA (https://sealevel.nasa.gov/ipcc-ar6-sea-level-projection-tool), as well as wave direction and significant height of waves (SHW) in 2022 were downloaded from the European Centre for Medium-Range Weather Forecasts (ECMWF) (https://cds.climate.copernicus.eu/cdsapp#!/home). Notably, due to the lack of measured water depth data, the GDEM data had not been corrected, and its value was only used as a reference for the relative elevation of the study area.

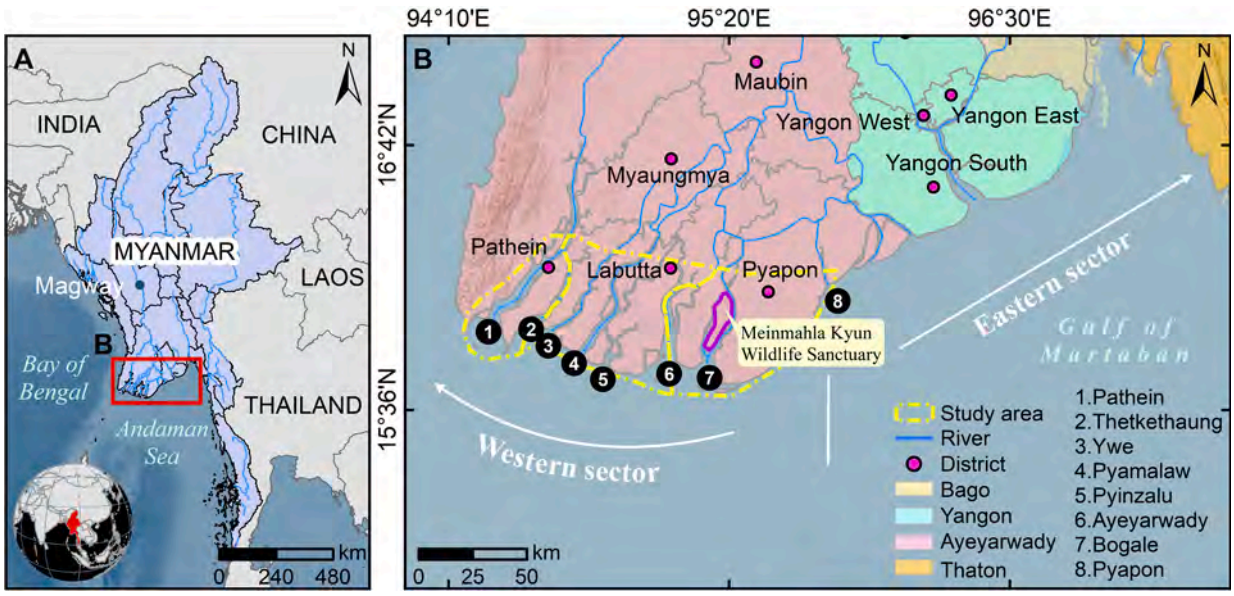


**Fig. 1.** Study area. (A) Location of the Irrawaddy Delta; (B) detailed elevation map of the Irrawaddy Delta. The base map is the Shuttle Radar Topography Mission Digital Elevation Data.

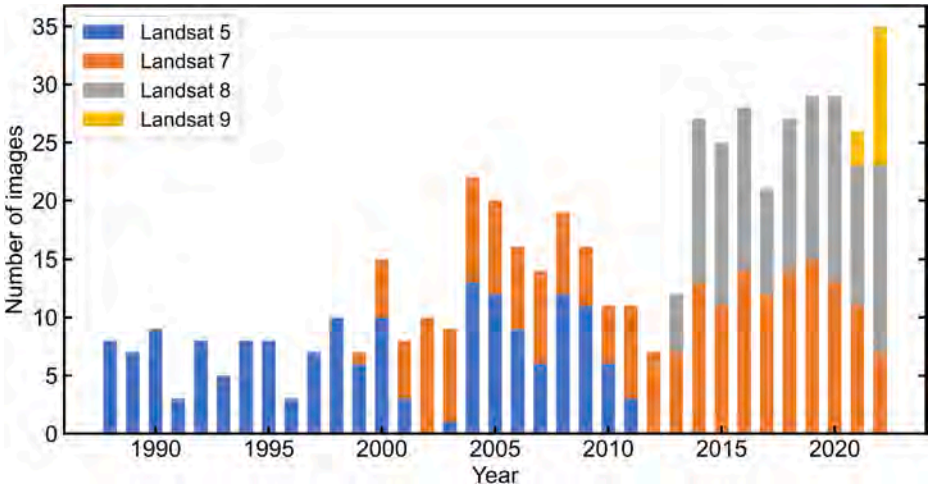


**Fig. 2.** The total number of satellite images.

### 2.3. Methods

#### 2.3.1. Computation of spectral indices

Various landforms have different spectral characteristics (Pike and Rozema, 1975). To adequately identify these spectral properties, in this study, the surface reflectances of blue, green, red, near-infrared, and shortwave infrared were chosen, and six spectral indices were calculated for each image on the GEE platform, such as the normalized difference vegetation index (NDVI) (Tucker, 1979), enhanced vegetation index (EVI) (Huete et al., 2002), land surface water index (LSWI) (Chandrasekar et al., 2010; Xiao et al., 2002; Xiao et al., 2004), modified normalized difference water index (mNDWI) (Xu, 2006), mangrove vegetation index (MVI) (Baloloy et al., 2020), and normalized difference mangrove index (NDMI) (Shi et al., 2016). NDVI and EVI can separate vegetation from soil and water, which has great advantages for vegetation information extraction and feature recognition. mNDWI can well distinguish water bodies, and MVI and NDMI can differentiate mangroves from non-mangroves and other non-vegetation covers (e.g., bare soil, water, and buildings). The formulas for calculating six spectral indices are as follows:

$$NDVI = \frac{\rho_{NIR} - \rho_{red}}{\rho_{NIR} + \rho_{red}} \quad (1)$$

$$EVI = 2.5\frac{\rho_{NIR} - \rho_{red}}{\rho_{NIR} + 6\rho_{red} - 7.5\rho_{blue} + 1} \quad (2)$$

$$LSWI = \frac{\rho_{NIR} - \rho_{SWIR}}{\rho_{NIR} + \rho_{SWIR}} \quad (3)$$

$$mNDWI = \frac{\rho_{green} - \rho_{SWIR}}{\rho_{green} + \rho_{SWIR}} \quad (4)$$

$$MVI = \frac{\rho_{NIR} - \rho_{green}}{\rho_{SWIR1} - \rho_{green}} \quad (5)$$

$$NDMI = \frac{\rho_{SWIR2} - \rho_{green}}{\rho_{SWIR2} + \rho_{green}} \quad (6)$$

where $\rho_{blue}$, $\rho_{green}$, $\rho_{red}$, $\rho_{NIR}$ and $\rho_{SWIR}$ represent the pixel values of the blue, green, red, near-infrared, and shortwave infrared bands of the

Landsat images, respectively.

#### 2.3.2. Random forest

The Random Forest (RF) algorithm, initially proposed by Breiman (2001), is a supervised machine learning method that consists of multiple decision trees (DTs). RF constructs individual DTs on randomly generated subsets of the original training set and combines them to form the final RF model. Randomly selecting features and samples during the training process, RF exhibits strong generalization capabilities and computational efficiency, making it suitable for datasets with heterogeneous categories. RF is widely employed in classification tasks involving multidimensional attributes (Tatsumi et al., 2015). Consequently, RF has demonstrated superior effectiveness in identifying mangrove forests compared to other algorithms (Mahdavi et al., 2018).

The combination of multiple spectral bands enhances the capability to distinguish different types of mangrove forests. In this study, the Random Forest (RF) algorithm was utilized to identify mangrove forests and shrimp ponds. Six spectral indices, namely NDVI, EVI, LSWI, mNDWI, MVI, and NDMI, along with the reflectance values of blue, green, red, near-infrared (NIR), and shortwave infrared (SWIR) bands from Landsat median synthesized images, were employed as input variables for the RF model. Four training sample classes were generated through visual interpretation, including mangrove forest, shrimp pond, seawater, and other land cover types, using datasets from Global Mangrove Watch, historical images from Google Earth, and composite images. The training dataset consisted of 80% of the samples, while the remaining 20% were used for model accuracy testing. Time series training samples were created at yearly intervals from 1988 to 2022 based on the training samples from 2022. Subsequently, the prepared images were classified into mangrove forests, ponds, seawater, and other land cover classes. Following the determination of the mangrove forest distribution and visual adjustments to ensure classification accuracy, maps depicting the changes in mangrove forests in the WIRD from 1988 to 2022 were obtained.

#### 2.3.3. Extraction of mangrove forests shoreline

The mangrove shoreline delineates the boundary between the dense forest cover of mangroves and the intertidal zone comprising tidal flats or seawater (Tran et al., 2014). In this study, the border pixels that distinguish mangrove, land, and sea were identified and designated as the mangrove shoreline. ArcGIS, a valuable software tool, facilitated various tasks such as geometric calculations, data visualization, spatial overlay analysis, and monitoring changes in ground objects. The mangrove shoreline was manually extracted using ArcGIS. Initially, the shoreline for the year 2022 was visually interpreted based on the composite image, with the seaward edge of the mangrove forest serving as an indicator. Subsequently, these interpreted results were superimposed onto the 2017 composite image and meticulously corrected segment by segment to manually digitize the mangrove border for the year 2017. Similarly, the positions of the mangrove shorelines for the years 1988, 1992, 1997, 2002, 2007, and 2012 were digitized using a similar approach of manual digitization.

#### 2.3.4. Spatial analysis of mangrove forests

To assess the change process of mangrove forests, the gain and loss of mangrove forests were quantified using the erase function within the overlay toolset in ArcGIS (Scott and Janikas, 2010).

The Digital Shoreline Analysis System (DSAS), an ArcGIS software extension developed by the United States Geological Survey (USGS), provides quantitative analysis of shoreline dynamics using various metrics. In this study, we manually extracted mangrove forest shorelines for the years 1988, 1992, 1997, 2002, 2007, 2012, 2017, and 2022 in ArcGIS based on the classification results. Subsequently, a total of 2,119 transects were generated, spaced 100 m apart and oriented perpendicular to the offshore baselines, to facilitate analysis. The Linear Regression Rate (LRR) was employed to examine the movement of mangrove forest shorelines over an eight-year period from 1988 to 2022. LRR calculates the slope of the least-squares regression line fitted to all shoreline points along a transect (Himmelstoss et al., 2021). This method considers all shorelines for analyzing long-term changes in mangrove shorelines (from 1988 to 2022), minimizing short-term variations and potential random errors (Wang et al., 2014). A negative rate indicates erosion (landward movement of the shoreline), while a positive rate signifies accretion (seaward movement of the shoreline).

The Net Shoreline Movement (NSM) and End Point Rate (EPR) were used to calculate the net change distance and movement rate of the oldest (1988) and youngest (2022) shorelines for each transect by DSAS (Himmelstoss et al., 2021). Then the formula for calculating the seaward gains of mangrove forests area of 1988 and 2022 ($Area_{gain}$) is as follows:

$$Area_{gain} = NSM_{EPR>0} D_T \tag{7}$$

where $NSM_{EPR>0}$ is the NSM when the shorelines of 1988 and 2022 move seaward ($EPR > 0$), and $D_T$ is the transect spacing (100 m in this study).

For comparing with sea level rise to determine the possible impacts of mangrove forests, the formula for calculating the average vertical sediment accumulation (AVSA) rate is as follows:

$$AVSA = V\tan\theta \tag{8}$$

where $V$ is the average accretion rate of shorelines, and $\theta$ is the average slope in the WIRD obtained from DEM.

#### 2.3.5. Landscape indices

The structural components and spatial organization of a landscape can be reflected in landscape indices, which condensed a great deal of information about landscape patterns (Wu, 2000; Zhang, 2008). Based on the classified mangrove forest patches, we calculated four landscape indices using MATLAB to study the spatial and temporal variations of mangrove forest landscape pattern: (1) The patch density (PD) is proportional to the degree of spatial heterogeneity and fragmentation of the landscape, indicating the degree of human disturbance to the landscape. (2) The largest patch index (LPI), which measures patch size and is inversely correlated with distribution dispersion, depicts patch shape. (3) The landscape shape index (LSI) is proportional to the degree of irregularity of the patch shape in the landscape. (4) The aggregation index (COHESION) represents the degree of natural cohesion between the same patch types, proportional to the degree of aggregation between the same patch types. The formulas are as follows (McGarigal and Marks, 1995):

$$PD = \frac{N}{A} \tag{9}$$

$$LPI = \frac{\max(a_i)}{A}(100) \tag{10}$$

$$LSI = \frac{E}{2\sqrt{\pi A}} \tag{11}$$

$$COHESION = \left[1 - \frac{\sum_{i=1}^{n} p_i}{\sum_{i=1}^{n} p_i \sqrt{a_i}}\right] \cdot \left[1 - \frac{1}{\sqrt{N}}\right]^{-1} (100) \tag{12}$$

where, i: 1, …, n patches, N: total number of patches in the landscape, ai: area of patch i, A: total landscape area, max: area of the largest patch in the landscape, pi: perimeter of patch i, E: total length of the edge in the landscape.

### 2.4. Accuracy assessment

Based on the data processing and resolution of the remote sensing images, the verification of the results obtained through remote sensing

images is crucial in ensuring their reliability (Heale and Twycross, 2015). Specifically, Given that the resolution of the Landsat image is 30 m, the spatial size corresponding to one pixel is only $9 \times 10^{-4}$ km$^2$, which is considerably smaller than the study area of this study (7,776.23 km$^2$). Consequently, it can be inferred that the impact of image resolution is negligible. In evaluating the classification of RF, the overall accuracy and kappa coefficient were employed (Prasad et al., 2022). The annual accuracy assessment of the RF-based classification is presented in Table S1. Notably, the overall accuracy and kappa coefficient of each year exceeded 0.98 and 0.96 respectively, indicating a high level of confidence in the classification outcomes derived from the RF model in this study, and the results obtained from the Landsat image can be considered reliable. Furthermore, a confidence interval of 90% was established for DSAS, serving as a weighted linear rate parameter. In addition, to improve the reliability of the results, a 95% confidence interval was constructed for the results while considering the bias of the linear interpolation method.

## 3. Results

### 3.1. Variations in mangrove forest area

From 1988 to 2022, the area covered by mangroves in the WIRD experienced a consistent annual decline (Fig. 3A), and the overall mangrove coverage decreased from 247,956.93 ha in 1988 to 135,498.69 ha in 2022. Over the past 35 years, the WIRD experienced a significant loss of 112,458.24 ha, which accounts for approximately 45.35% of the total mangrove forests. The rate of decrease in the WIRD's mangrove forests area was calculated to be 1.86% per year. However, it's important to note that this trend was not consistent throughout the entire study period. The change in mangrove cover area in the WIRD can be divided into two distinct stages (Fig. 3A). During the period from 1988 to 2005, there was a rapid reduction in mangrove cover, with an average annual change rate of −6,982.55 ha. This resulted in a loss of approximately 45.60% of the mangrove cover compared to the initial measurement in 1988. From 2005 to 2022, a fluctuating trend in mangrove cover emerged, characterized by an average annual variation of −49.75 ha. The overall loss during this period amounted to approximately 0.45% of the mangrove forests compared to the measurement in 2005 (Fig. 3A).

The changes in mangrove areas within different regions of the WIRD exhibited distinct patterns (Fig. 3B-D). Initially, in 1988, the mangrove area in Pathein, Labutta, and Pyapon accounted for 6.29%, 39.46%, and 54.25% of the total region, respectively. However, by 2022, there were notable variations in these proportions. Specifically, the mangrove area in Pathein increased to 10.92% (Fig. 3B), in Labutta it decreased to 36.65% (Fig. 3C), and in Pyapon it decreased to 52.43% (Fig. 3D).

Between 1988 and 2005, the mangrove area in Pathein underwent a substantial reduction from 15,601.29 ha to 10,315.80 ha, with an average annual rate of −336.31 ha. However, after 2005, the mangrove area began to increase at an average annual rate of 181.49 ha, reversing the previous trend (Fig. 3B) between 2005 and 2022. In Labutta, the mangrove area decreased from 97,850.42 ha in 1988 to 49,656.78 ha in 2022. Similarly, the area of mangroves shrank at rates of 2,669.43 ha/year from 1988 to 2005 and increased at rates of 2,669.43 ha/year from 2005 to 2022 (Fig. 3C). In Pyapon, the mangrove area decreased from 134,505.22 ha in 1988 to 71,042.94 ha in 2022. Conversely, the change pattern of the mangrove area in Pyapon mirrored that observed in the entire WIRD region between 1988 and 2005. During this period, the mangrove area in Pyapon decreased at rates of 3,976.81 ha/year. Furthermore, between 2005 and 2022, the decreasing trend in mangrove areas was alleviated, with the change rates in Pyapon being

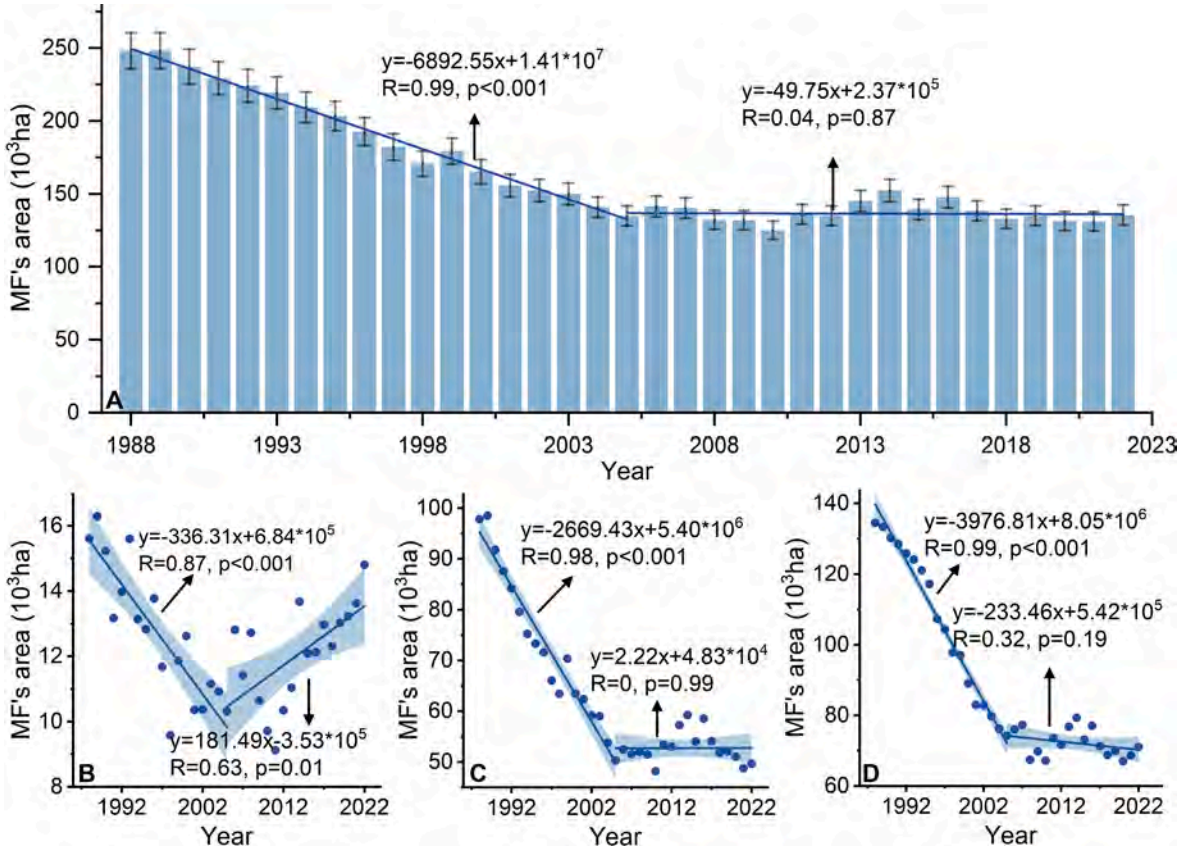


**Fig. 3.** Temporal variation of mangrove forest (MF) area in the WIRD. A: Time variation of the total mangrove forest area. B-D: represents the temporal variation of mangrove area in Pathein, Labutta and Pyapon, respectively.

−295.14 ha/year (Fig. 3D). The mangrove area in Labutta experienced a decline of 49.25%, while in Pyapon, the mangrove area decreased by 47.18%.

### 3.2. Gain and loss in mangrove forest area

Between 1988 and 2022, Pathein, Labutta, and Pyapon exhibited distinct spatial patterns of gain and loss in mangrove forest areas within the WIRD (Fig. 4). During this period, the overall trend in the WIRD's mangrove forests was a decline. Specifically, from 1988 to 1992, significant losses of mangrove forests were observed near the Labutta-Pyapon border, as well as on the edges of southern Labutta and estuarine sandbanks. On the other hand, mangrove expansion occurred in northern Labutta and along the margins of several river sandbars. Southern Pathein experienced a combination of mangrove expansion and reduction (Fig. 4A). Overall, between 1988 and 2022, the total gains in mangrove forest area amounted to 27,851.54 ha, while losses accounted for 146,323.80 ha. Notably, the gained areas toward the sea compensated for a loss of 2,812.32 ha (Table S2).

From 1992 to 1997, the mangrove forest area experienced significant losses, with a total damage of 57,668.26 ha observed across the three zones (Fig. 4B, 4H; Table S2). In addition to the previously expanding areas, the mangrove forests near the Labutta-Pyapon border suffered extensive depletion. Furthermore, substantial losses of mangrove forests were observed in southern Pathein and the eastern region of Pyapon. However, some areas showed positive growth of mangrove forests, such as a small isolated island located between the river channels in the middle of Labutta and the land near the southern river channel of Labutta and Pyapon (Ayeyarwady estuary). The mangrove forests also demonstrated growth along the land margins and the sandbanks (Fig. 4B).

Between 1997 and 2002, there was widespread destruction of pre-existing mangrove forests in eastern Pyapon. Losses of mangrove forests continued in southern Pathein and migrated from the north to the south of the Labutta-Pyapon border. However, there was a significant gain of mangrove forests in western Labutta, and continuous growth was observed in the central region of Labutta. Estuary sandbanks, river sandbanks, and the southern land on the outer margin, such as western Pathein and southern Meinmahla Kyun Wildlife Sanctuary, exhibited notable gains in mangrove area (Fig. 4C). Subsequently, from 2002 to 2007, the loss of mangroves was mitigated, with a decrease of 39,979.20 ha (Fig. 4D, 4H; Table S2). Although there was a substantial loss of 20,036.91 ha in Pyapon, particularly in the west and south, it was largely offset by a gain of 14,527.60 ha in the east (Table S2). Additionally, during this period, mangrove areas started to expand near the channels of Labutta, on the southern land of Pathein, and at the edges of estuarine sandbanks, while the interior of southern Labutta remained severely damaged (Fig. 4D). Between 2007 and 2012, significant losses

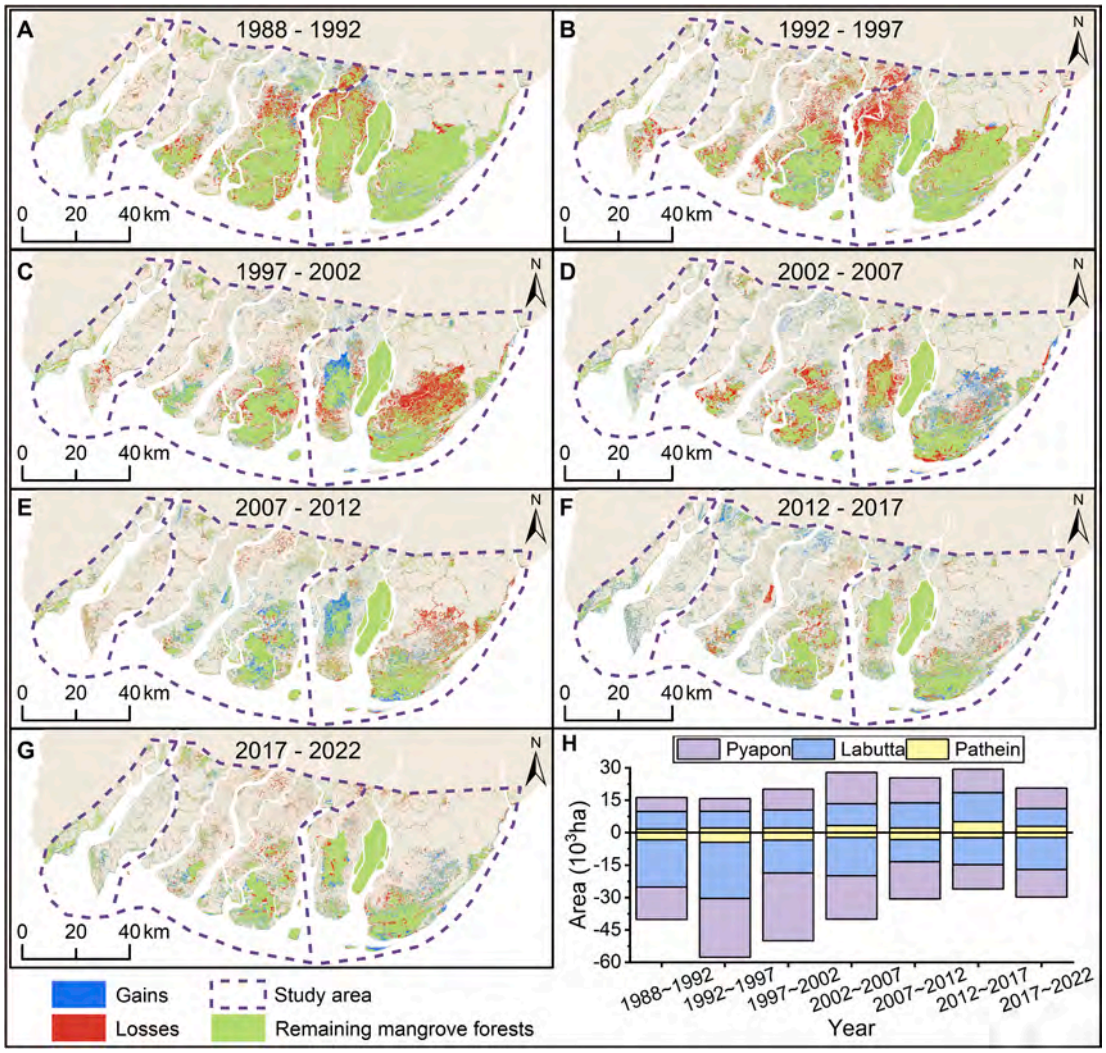


**Fig. 4.** Gains and losses of mangrove forest area in the WIRD. A-G: Spatial distribution of mangrove forests during 1988–2022. H: loss and gain areas of the seven periods. Green refers to the mangrove extent in the beginning year of this period.

of mangrove forests occurred in eastern Labutta, including its land interior and eastern coast. Conversely, while mangrove forests were lost once again in southern Pathein and northern Labutta, there was an improvement in the southwestern region of Labutta, where mangrove forests had previously declined. Furthermore, there was a considerable gain of mangrove forests at the land margin of the Labutta-Pyapon border and the southwestern Pyapon. Scattered patches of mangrove forests formed along the land margin near the river channel, while mangrove forests eroded at the estuary sandbanks closer to the sea (Fig. 4E).

Furthermore, there was a significant increase in the mangrove forest area between 2012 and 2017, with the emergence of new mangrove forests covering 29,420.68 ha across the three zones (Fig. 4F, 4H; Table S2). The majority of this growth occurred in southern Pathein, northern Labutta, and southeastern Pyapon, along the land margins near river channels, and estuarine sandbanks. However, the mangrove forests in southern Labutta sustained permanent damage, experiencing a loss of approximately 26,034.33 ha (Table S2). Additionally, losses were observed mainly in southeastern Labutta and the interior of Pyapon, excluding the Meinmahla Kyun Wildlife Sanctuary. Despite these losses, the overall mangrove forest areas in these three regions exhibited net gains (Fig. 4F).

Moreover, there was a notable expansion of mangroves primarily along the outer edges of the WIRD, as well as on both sides of river channels and estuarine sandbanks between 2017 and 2022, while losses continued to be scattered within the inland areas (Fig. 4G). Overall, the mangrove forests in the WIRD underwent significant spatial changes over the past 35 years, characterized by increasingly fragmented patches of mangroves and limited connectivity. The gain in mangrove area predominantly occurred in the seaward regions, while the loss was primarily observed in the landward areas.

### 3.3. Shoreline change in mangrove forest

While some shorelines in the WIRD exhibited landward movement, the mangrove forest shorelines displayed a general seaward trend, with an average overall migration rate of 0.26 m/yr between 1988 and 2022, as determined through shoreline analysis of 2,119 transects (Fig. 5A). The expansion and erosion sections of the shorelines accounted for approximately 50% each, with change rates of 7.65 m/yr and −7.09 m/yr, respectively (Fig. 5B). The maximum expansion rate and the maximum erosion rate were 49.85 m/yr and −46.36 m/yr, respectively. Specifically, the shoreline of the Pathein mangrove forest exhibited a predominantly seaward movement over the past 35 years, with an average rate of change of 0.90 m/yr. Transects characterized by progradation (shoreline advancement) and erosion accounted for 65.60% and 34.40% of the Pathein area, respectively. The Pathein mangrove forest experienced a relatively limited range of change in its shoreline, with expansion and erosion shorelines alternating and the maximum rate of change remaining below 20 m/yr (Fig. 5B).

The Labutta mangrove forest shorelines were characterized by a predominant landward retreat, with a mean rate of change of −1.50 m/yr, indicating a faster alteration compared to Pathein. Within Labutta, erosion and expansion accounted for 42.59% and 57.41% of all transects, respectively. Key areas where the mangrove shoreline experienced erosion included the east side of the Thetkethaung River, both sides of the Ywe River, both sides of the Pyamalaw River, and the west side of the Ayeyarwady River. On the other hand, expansion primarily occurred behind the non-barrier island on the southeast side of Labutta (Fig. 5A).

The Pyapon mangrove shorelines demonstrated a seaward expansion

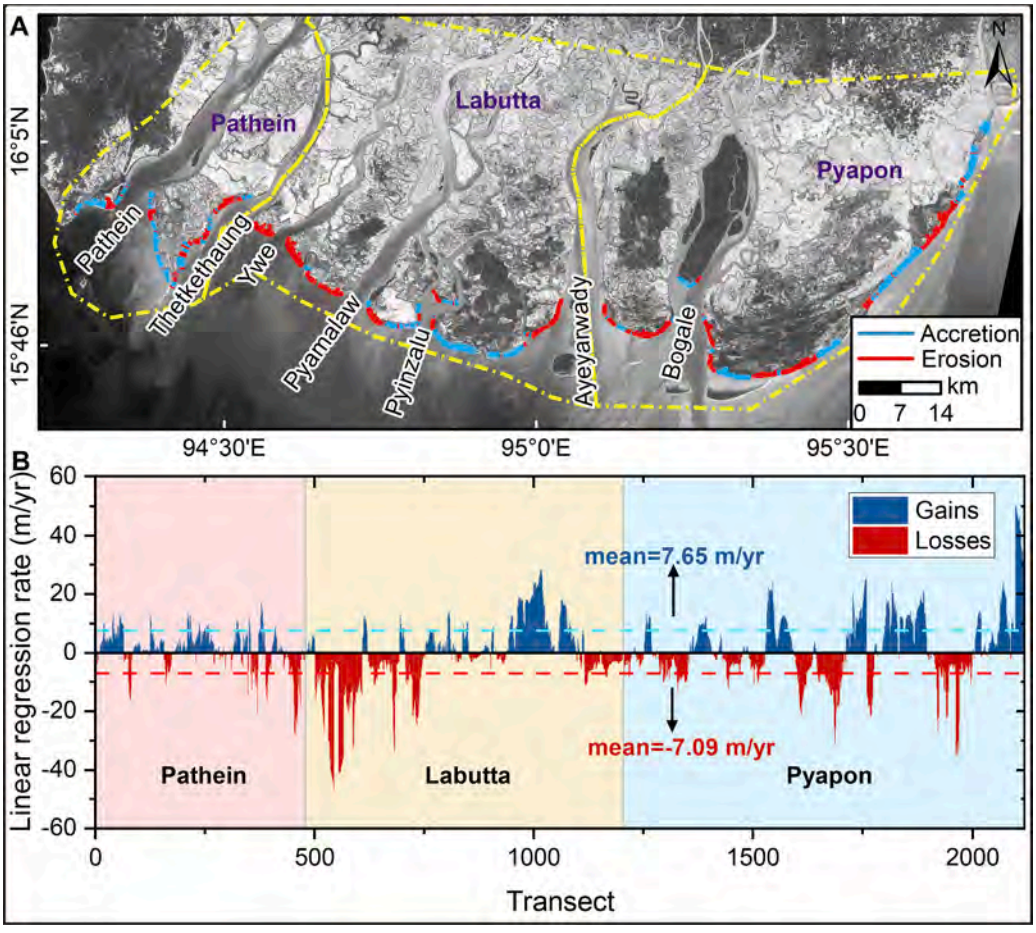


**Fig. 5.** Movement of mangrove forest shorelines in the WIRD.

rate of 1.27 m/yr, with 46.89% of transects showing expansion and 53.11% showing erosion. These shoreline changes in Pyapon were significantly more severe compared to Pathein. The erosion of the mangrove shoreline predominantly occurred on the east side of the Ayeyarwady River, both sides of the Bogale River, and the east and southeast sides of Pyapon. Conversely, mangrove encroachment primarily took place on the south side of Meinmahla Kyun Wildlife Sanctuary, the southeast side of Pyapon behind the barrier island, and the east side of Pyapon (Fig. 5A).

### 3.4. Landscape pattern change in mangrove forest

The landscape structure and its changes can provide insights into the combined influence of various abiotic and biotic factors, both natural and human-induced, and their ecological consequences. In this context, the analysis of mangrove patch landscape indices reveals distinct patterns across different regions over the past 35 years (Fig. 6). Specifically, the mangrove landscape PD exhibited an overall increasing trend, with PD values rising from $1.01*10^{-5}$ in 1988 to $1.29*10^{-5}$ in 2022 (Fig. 6A). The PD of Pathein, Labutta, and Pyapon also displayed increasing trends, with growth rates of $1.54*10^{-7}$, $5.55*10^{-7}$, and $5.41*10^{-7}$, respectively (Fig. S2A1, S2B1, S2C1). In summary, the patch density of the mangrove landscape in the study area exhibited a consistent upward trend from 1988 to 2022 indicating an increase in both the degree of mangrove landscape fragmentation and landscape heterogeneity.

The COHESION analysis of mangrove patches revealed a general declining trend over time. The value of COHESION decreased from 99.98 in 1988 to 99.95 in 2022 (Fig. 6B). Except Pathein, both Labutta and Pyapon also experienced annual declines in COHESION, with rates of change recorded at $-3.23*10^{-7}$, $-1.86*10^{-5}$ and $-1.18*10^{-5}$, respectively (Fig. S2A2, S2B2, S2C2). These findings suggest that the mangrove patches are becoming increasingly dispersed, indicating a reduction in the overall interconnectedness and spatial continuity of the mangrove landscape.

Moreover, the LPI displayed a declination, which increased from 0.25 in 1988 to 0.29 in 1994 and then fell to 0.08 in 2001, respectively (Fig. 6C). The LPI of Pathein ($9.51*10^{-4}$) increased yearly, except for Labutta ($-5.09*10^{-6}$) and Pyapon (-0.01) (Fig. S2A3, S2B3, S2C3). Mangrove patches in the study area were continuously fragmented from 1988 to 2022.

The LSI was 133.99 in 1988, increased to 229.85 in 2015, and dropped to 122.89 in 2022 (Fig. 6D). Along with rising year over year, the LSIs of Pathein, Labutta, and Pyapon did as well, with growth rates of 0.17, 0.89, and 1.51, respectively (Fig. S2A4, S2B4, S2C4). The LSIs have gradually increased in the last 35 years, indicating that the mangrove patch shape has become more complex and irregular.

## 4. Discussion

### 4.1. Impacts of suspended sediment discharge from upstream

The transport of suspended sediment discharge (SSD) by rivers plays a crucial role in facilitating the accumulation of tidal flats within deltas, thereby creating new physical spaces that promote the growth of mangroves (Swales et al., 2019). Several studies have indicated that wetlands in river deltas, particularly the Mississippi and Ganges deltas, may experience reduced growth rates or complete disappearance due to declines in SSD and water supply to the wetlands, as well as rapid subsidence of the delta itself (Edmonds et al., 2023; Jayanthi et al., 2023; Lovelock et al., 2021). However, recent research has revealed an intriguing finding: despite a clear decline in SSD originating from upstream sources, the mangrove forest shoreline in the Red River delta has exhibited continued seaward advancement (Long et al., 2021). At the Meinmahla Kyun Wildlife Sanctuary, an inner distributary mouth area, mangroves effectively developing due to its multiple pathways (Glover et al., 2022). The slow rate of progradation (0.26 m/yr) of the mangrove

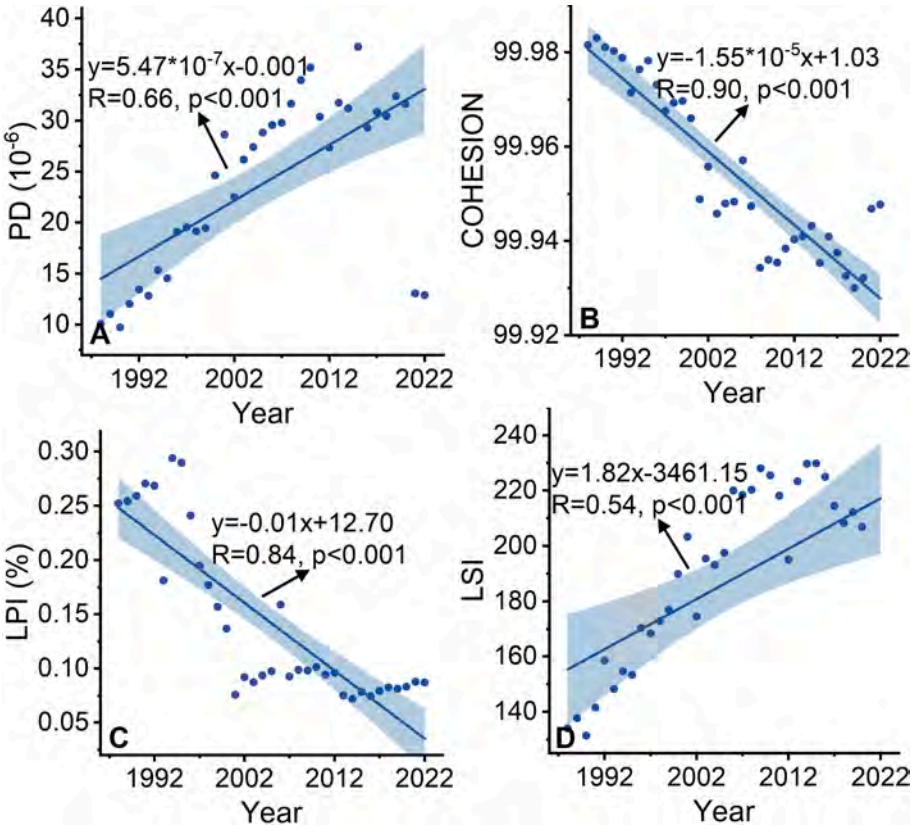


**Fig. 6.** Landscape indices changes of mangrove forest in the WIRD. A-D: PD, COHESION, LPI, and LSI.

forest shoreline appears to be partially due to that the majority of the sediments carried by the Ayeyarwady River's is accumulating in the Gulf of Martaban instead of the WIRD, leading the delta shoreline to gradually prograde (Hedley et al., 2010).

Moreover, we conducted correlation analyses between SSD at the Magway station and mangrove forest area in the WIRD and its sub-regions from 1990 to 2010. The results showed that only the correlation coefficient between SSD and mangrove forest area in Pyapon exceeded 0.4, indicating a potential influence of SSD on mangrove dynamics in that specific region. However, for the overall WIRD and the Pathein and Labutta sub-regions, the correlation coefficients did not reach statistical significance, suggesting that the gain and loss of mangroves in these areas may not be strongly influenced by the SSD entering the sea. The Pathein River, located approximately 248 km south of the Magway site, serves as a smaller distributary of the Irrawaddy River in the westernmost part of the delta (Fig. 1B). This region receives a relatively lower amount of SSD from upstream mountain rivers, resulting in a lesser impact on the mangroves in Pathein. In contrast, the Labutta

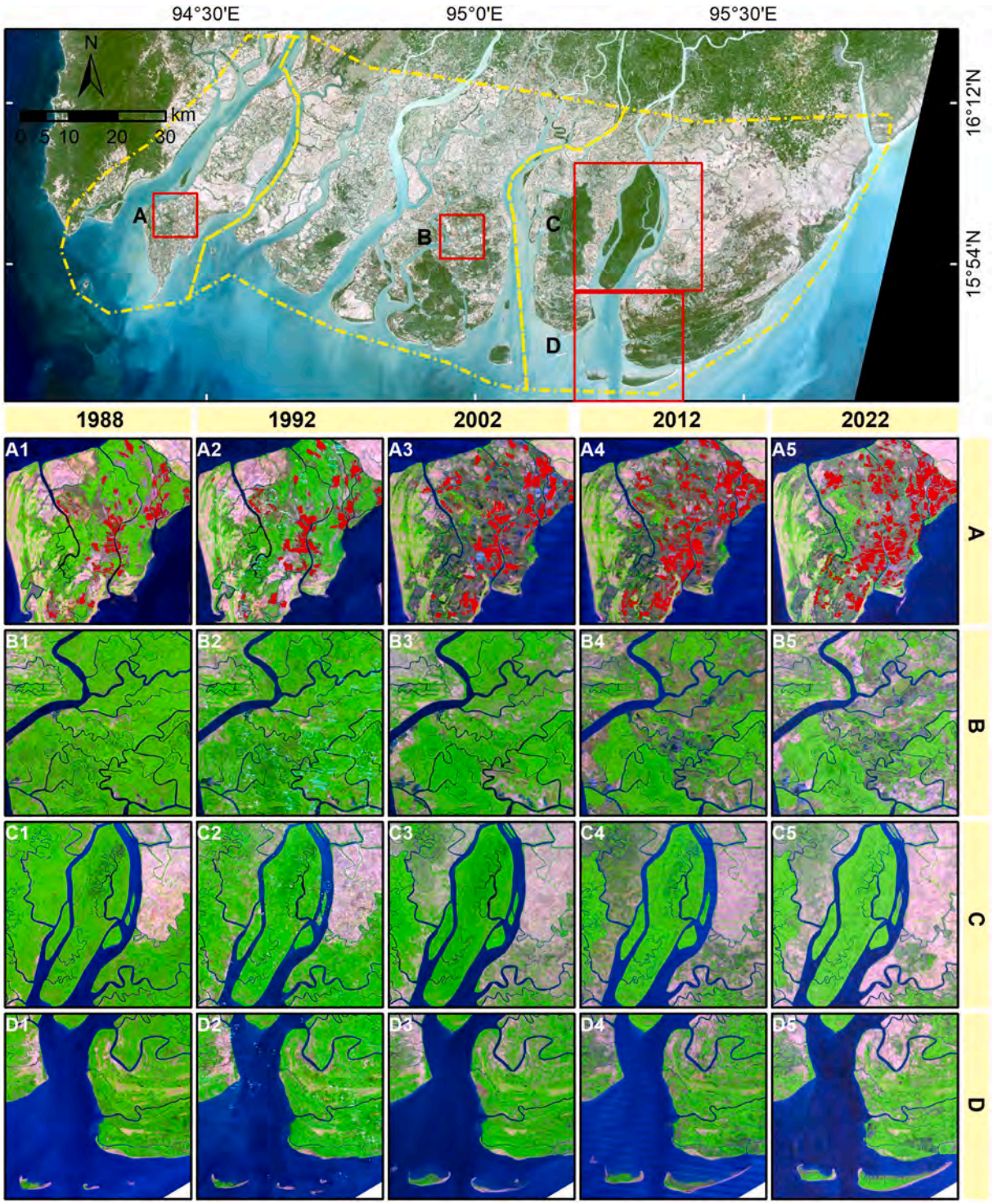


**Fig. 7.** Temporal and spatial changes of mangrove forests in the WIRD. Green is mangrove forest, pink is bare land, blue is water, and the red part of A is shrimp ponds.

sub-region, situated in the middle of the delta, exhibits more pronounced meandering compared to the eastern Pyapon sub-region (Fig. 1B). This meandering pattern leads to weaker riverine hydrodynamics along the Labutta channel, promoting sediment deposition within the river channel itself. Consequently, only a minor proportion of the upstream SSD reaches the delta front in Labutta, while Pyapon receives direct SSD inputs through the Ayeyarwady River into the eastern part of the WIRD. These observations suggest that Pyapon is more likely to be regulated by SSD inflow compared to Labutta. Therefore, the expansion of the mangrove forest in the Pyapon estuary can be partially attributed to the influence of SSD from upstream sources. However, the overall gain and loss of mangroves in the entire WIRD may have less significant impacts resulting from upstream SSD movements.

To further understand the relationship between SSD and mangrove dynamics in the WIRD, it would be beneficial to quantify the correlation between SSD at each fork of the delta and the gain and loss of mangroves. This would require additional observations of sediment flux into the sea at each fork, providing more comprehensive insights into the influence of upstream SSD on the mangrove ecosystem.

### 4.2. Impacts of anthropogenic activities

The loss of vegetation in Yangtze River Delta and Yellow River Delta are both primarily attributed to intensive human activities (Chang et al., 2022; Qu et al., 2018). Extensive deforestation, driven by the advancements of human civilization, has led to the conversion of mangrove forests into alternative land-use types, making it the primary cause of the significant decline in mangrove forests (Goldberg et al., 2020; Hagger et al., 2022). As one of Myanmar's most densely inhabited regions (Furuichi et al., 2009), mangrove forests in the WIRD suffered man-made adverse effects as evidenced by the growing level of fragmentation revealed by the landscape indices (Fig. 6, S2A1). To illustrate the land-use changes in mangrove forests, Fig. 7 presents the transitions in four regions that have experienced substantial degradation. In the southwestern part of the WIRD, some mangrove forests have disappeared during the study period due to their conversion into shrimp ponds, particularly in Pathein. The remaining mangrove patches in Pathein have become isolated due to the expansion of aquaculture ponds, resulting in progressive fragmentation. Shrimp aquaculture in the WIRD began in the 1970 s.

Following the implementation of government policies aimed at promoting economic growth, the aquaculture industry experienced significant development, leading to the establishment of shrimp and fish ponds for global trade (Filipski and Belton, 2017). The expansion of shrimp pond areas during the 1990 s was driven by these economic initiatives, and a subsequent decline occurred in 2004, as depicted in Fig. 8. Interestingly, this change in shrimp pond areas coincided with a corresponding trend in mangrove areas in the WIRD. From 1989 to 2005, the rapid expansion of shrimp pond areas was accompanied by a loss of mangrove forests. Conversely, between 2005 and 2022, there was a decrease in shrimp pond areas alongside an increase in mangrove forest coverage. In terms of the overall impact, shrimp pond areas accounted for 2.26% of the total mangrove loss in 1988, a figure that rose to 3.82% by 2022. This indicates a growing contribution of shrimp pond expansion to the reduction of mangrove areas over time.

Moreover, agriculture expansion and urban development remain the primary drivers of mangrove forest loss. WIRD in Myanmar serves as a significant agricultural region, which provided approximately 85% of the charcoal consumed in the capital Yangon between 1971 and 1993 (Burma. Ministry of Forestry and Kokusai Kyōryoku Jigyōdan, 2005). Historical records indicate that mangrove forests in the WIRD suffered extensive deforestation and conversion to agricultural land during the period from the 1870 s to the 1880 s, primarily driven by the increasing demand for resources in urban areas (Ono, 2007). As depicted in Fig. 7B, significant removal of mangrove forests can be observed in eastern Labutta, an area that experienced the most substantial loss of mangrove forests. This clearance of mangrove forests was undertaken to pave the way for the establishment of bare or agricultural land. The results of other land area from 1988 to 2022 (Fig. 9) show that the area changes of agricultural and urban land are both highly consistent with the dynamic of mangrove forests area while that of shrimp ponds indicates an insignificant correlation, suggesting that agriculture expansion and urban development play a more prominent role than shrimp pond expansion on the mangrove forests area variation.

Since its establishment in 1986, the Meinmahla Kyun Wildlife Sanctuary has served as a crucial protective measure for mangrove forests, allowing them to grow naturally. Within the sanctuary, the mangrove forests have been adequately conserved, providing a contrasting scene of lush greenery in contrast to the barren pink landscape of deforested areas (Fig. 7C). Unfortunately, outside the boundaries of the Meinmahla Kyun Wildlife Sanctuary, mangrove forests have suffered extensive degradation and deforestation, and these non-protected areas have experienced a significant reduction in mangrove forest coverage, resulting in their decimation.

### 4.3. Impacts of ocean dynamics

Undeniably, the phenomenon of sea level rise due to global warming is prevalent in the WIRD (IPCC, 2022), including a sea level rise rate of 3.53 mm /yr (Fig. 10). Given the large-scale sea level rise, mangrove forests are being forced to migrate landward (Gilman et al., 2007; Liang et al., 2022; Mafi-Gholami et al., 2020). However, our results demonstrated a noteworthy expansion of the shoreline towards the sea on the southeastern side of the delta, and this expansion is particularly evident in Pathein and Pyapon, with rates reaching 4.27 m/yr and 10.48 m/yr, respectively (Fig. 5B). Approximately 2,812.32 ha of mangrove forest in the WIRD are thriving in the seaward direction. Furthermore, the

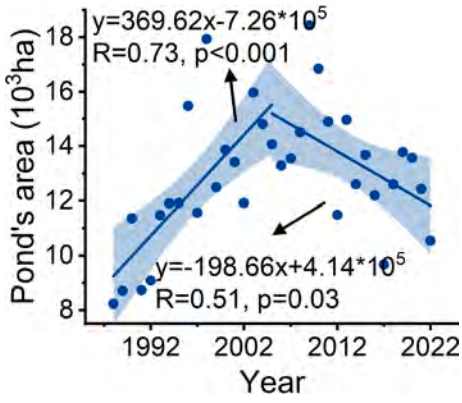


**Fig. 8.** Area of shrimp ponds from 1988 to 2022.

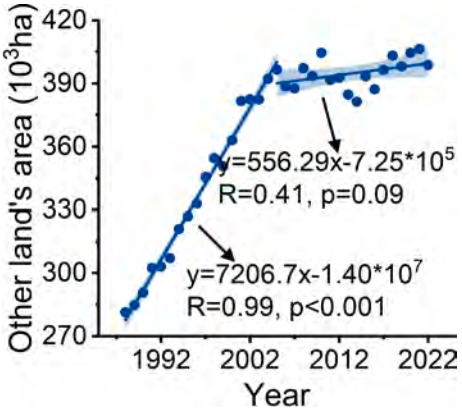


**Fig. 9.** Area of other land from 1988 to 2022.

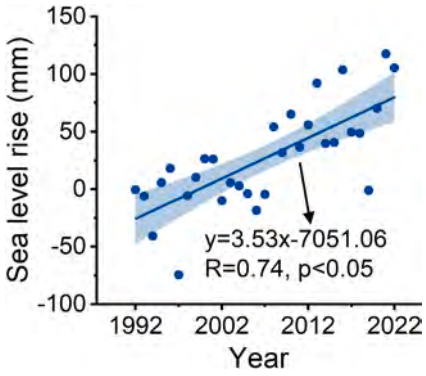


**Fig. 10.** The sea level rise and its simple linear regression analysis from 1988 to 2022.

average vertical sediment accumulation rate calculated from the average slope in the WIRD is 84.12 mm/yr, which exceeds the rate of sea level rise. This suggests that, currently, sea level rise may not pose an immediate risk to mangrove forests in the WIRD. However, it is important to note the presence of eroding shorelines within the area.

Meanwhile, waves exceeding 1 m in height (Fig. 11A) is a crucial factor in shaping the delta. mangrove forests, which thrive in shallow coastal waters, are vulnerable to waves (Spalding et al., 2014; Xie et al., 2022). The erosion of mangrove forest shorelines can be attributed to persistent strong waves (Long et al., 2021). The regional southwest wave, influenced by the southwest monsoon, occurs with a frequency exceeding 60%. Waves ranging from 0.5 to 1 will continue to strike the shore under the influence of the monsoon, pushing shoreline landward retreat, particularly in the southwestern Labutta area. Over 41.67% of the southwest waves have a significant wave height surpassing 1 m (Fig. 11A). As a result, the sediment surrounding the mangrove roots is eroded, exposing them to waves over 1 m high and resulting in uprooting and loss of the mangroves. Erosion is also observed along the southwest coast of the WIRD, which is similar to the mangrove forest shoreline around Qinzhou Bay, China (Fig. S3).

Furthermore, the presence of sandbanks and barriers at the estuary plays a crucial role in protecting mangrove forests from the energy of large waves and tides, providing a favorable environment for their growth (Long et al., 2021). Particularly, the development of a barrier island in the Pyapon estuary demonstrates a high capacity to withstand powerful waves, allowing sediment carried by wave overwash to accumulate in the shallow water behind the barrier island. This accumulation creates a conducive environment for the expansion of mangroves. Similar dynamics can be observed in the Red River estuary (Long et al., 2021). The barrier island effectively attenuates waves exceeding 1 m, resulting in reduced hydrodynamic energy in the area behind it. Consequently, the weakened waves no longer hinder the flourishing and seaward expansion of mangrove forests (Hu et al., 2022; Huang et al., 2021).

Similarly, the southwest wave can transport fine sediment particles suspended in the water to the back of the barrier island through wave overwashing, especially during periods of relatively low tidal water levels when wave energy is dissipated by the presence of the barrier island. As a result, the elevation of shallow tidal flats behind the barrier island can be raised, creating favorable conditions for the colonization of mangroves. However, the sandy shoreline experiencing landward retreat in the eastern Pyapon area exposes the back barrier to wave action, leading to further erosion of the mangrove shoreline (Anthony et al., 2019).

Furthermore, the WIRD is prone to frequent tropical cyclones, which contribute significantly to the high occurrence (41.67%) of waves exceeding 1 m in height. One notable example is the tropical Cyclone Nargis, which occurred from May 2–4, 2008, and was considered the strongest meteorological event to impact the delta in recent decades (Fritz et al., 2009). With wind speeds reaching 215 km/h, Cyclone Nargis caused extensive devastation and is regarded as one of Myanmar's deadliest natural disasters in recorded history. The Delta region, being subjected to a 4-meter storm surge, experienced the most severe damage (Nanda, 2014). After Nargis, the WIRD witnessed a decrease in mangrove cover attributed to the cyclone (Win et al., 2020). Additionally, shoreline retreat, as indicated by the high-water line used as a proxy, was observed in the same year (Besset et al., 2017). However, before the cyclone, the mangrove shoreline had been advancing seaward at a rate of 2.93 m/yr from 2007 to 2012. The mangrove forest area also experienced a decrease of 5.76% from 2007 to 2008, followed by a minor decrease of 0.17% from 2008 to 2009 (Fig. 3 and Fig. 5). The destructive impact of the cyclone resulted in significant damage to many mangrove forests and altered the physical structure of the shoreline, raising global concerns. Considering the projected increase in the intensity of cyclones due to global warming, the mangrove ecosystems are likely to face continued destruction with limited resilience (Besset et al., 2017).

### 4.4. *Prospective*

The findings highlight that mangrove forests in the WIRD have experienced significant decline as a result of increased human activity, sea level rise, changes in sediment and water supply, and hydrodynamic changes. These cumulative pressures have put the remaining mangroves at great risk. It is crucial to prioritize the protection and conservation of

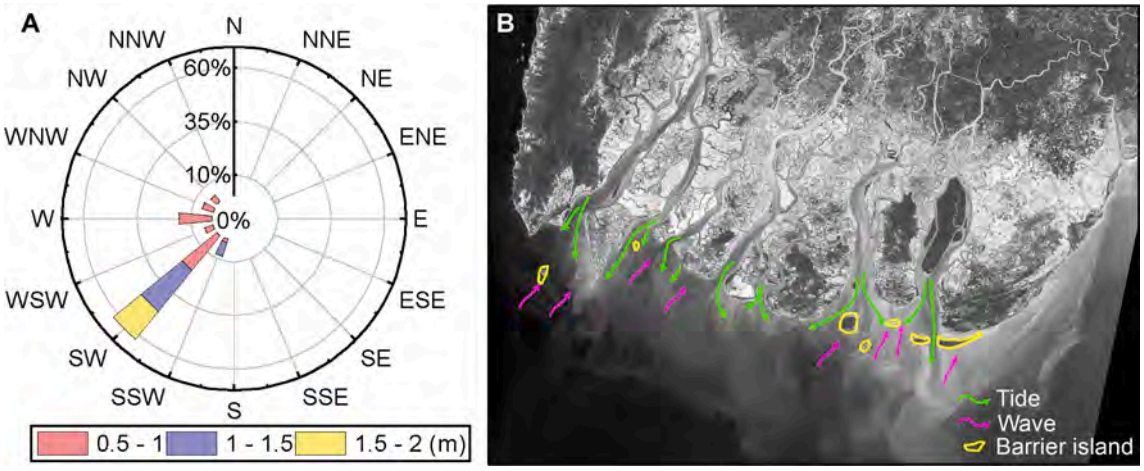


**Fig. 11.** A: Wave characteristics of the WIRD. B: Flow track diagram of suspended sediment affected by ocean dynamics.

the remaining mangrove forests, considering their ecological importance and the services they provide. Without effective mitigation measures, the loss of mangrove habitats and the decline of ecosystem services are inevitable outcomes (Bryan-Brown et al., 2020). Safeguarding these mangrove ecosystems is paramount to ensure their continued existence and the benefits they offer to both the environment and human communities.

Mangrove forests in the WIRD have undergone indiscriminate conversion into paddy fields without adequate consideration for coexistence with agriculture (Estoque et al., 2018). The extensive cutting of mangroves, particularly in Labutta and Pyapon, has led to significant losses of mangrove forests on the land portion. Additionally, mangroves have been converted into brackish shrimp ponds in the Pathein and southwest Labutta regions, further exacerbating the loss resulting from agricultural activities (Zöckler et al., 2013). However, it has been observed that mangrove forest in the WIRD area has experienced a decline followed by stabilization. To mitigate further losses, it is imperative to implement policies that enforce zoning regulations, thereby restricting additional land reclamation and urban development in critical mangrove areas. Furthermore, promoting sustainable agricultural practices that minimize the conversion of wetlands into farmland represents a crucial mitigation strategy.

Drawing inspiration from the success of the Meinmahla Kyun Wildlife Sanctuary, which has maintained a relatively stable mangrove forest (mangrove forest) area (Fig. 7C), it is imperative to establish protected areas in the remaining large contiguous mangrove areas, such as southeastern Labutta, western Pyapon, and southeastern Pyapon. These protected areas would safeguard the critical mangrove ecosystems from further degradation and loss. However, the increased risk of inundation due to sea-level rise and extreme weather events, exemplified by Cyclone Nargis, poses significant threats to mangroves (Dahdouh-Guebas et al., 2022; Lovelock et al., 2015). As the WIRD experiences a coexistence of seaward erosion and accretion, urgent action is needed to develop and implement adaptation strategies that specifically address the impacts of sea-level rise on mangrove forests, particularly along the southwest coast of the WIRD (Waryszak et al., 2021). Furthermore, implementing large-scale mangrove restoration projects that involve the replanting of native mangrove species, along with the use of natural or artificial structures such as gabions and bamboo fences, can help prevent erosion and provide protection for newly established mangrove forests (Mai Van et al., 2021; Huang et al., 2021). Additionally, considering controlled water diversion and sediment management strategies in estuaries and coastal rivers can facilitate self-regulation and maintain the natural hydrological balance in delta regions as a response to SLR (Alizad et al., 2018). To ensure the success of these initiatives, ongoing monitoring and evaluation are crucial. This will enable timely adjustments to be made as conditions change in the WIRD, allowing for adaptive management and the effective conservation of mangrove ecosystems.

## 5. Conclusions

The mangrove forests in the WIRD hold significant importance as a part of South Asia's mangrove ecosystems. The dynamics of mangrove forests in the WIRD exhibit considerable variations, and this study aims to provide a comprehensive assessment of the gain and loss of the WIRD's mangrove forests from 1988 to 2022. The major findings of the study are as follows:

1. Throughout 1988–2022, the total area of the WIRD's mangrove forests gradually decreased by 45.35%, corresponding to an annual decline of 1.86%. The area of Pathein and Labutta mangroves initially decreased before 2005 but showed an increasing trend between 2005 and 2022. In contrast, the mangrove areas in Pyapon experienced rapid declines with fluctuations. Specifically, the mangrove forest area of Pathein and Labutta decreased initially and then increased, while Pyapon witnessed rapid declines with fluctuating patterns.
2. The mangrove forests in the WIRD suffered from severe fragmentation, with mangrove forest patches becoming increasingly scattered. Moreover, the shorelines of the mangrove forests moved seaward at a rate of 0.26 m per year. Notably, the southwest region experienced erosion, while expansion was observed in the southeast. The progradation of 2,812.32 ha partially offset the overall loss of mangrove forests.
3. Deforestation for aquaculture ponds emerged as the primary cause for the significant degradation of the interior portions of mangrove forests. The continuous erosion in the southwest and seaward expansion in the southwestern mangrove forest shorelines were most likely influenced by large waves from the southwest monsoon. However, sea-level rise and sediment supply dynamics made minor contributions to the expansion and decline of mangrove forests. The seaward expansion of mangrove forests was facilitated by the presence of estuarine barriers, which provided sheltered conditions supporting mangrove habitats along the shorelines.

These findings shed light on the changing dynamics and challenges faced by the mangrove forests in the WIRD. Deforestation for aquaculture, erosion, and wave action have emerged as primary drivers of mangrove forest degradation, while estuarine barriers play a crucial role in supporting the expansion and preservation of mangrove forests. Understanding these dynamics is vital for implementing effective conservation and management strategies to safeguard the resilience and ecological functions of the WIRD's mangrove forests.

## Declaration of Competing Interest

The authors declare that they have no known competing financial interests or personal relationships that could have appeared to influence the work reported in this paper.

## Data availability

Data will be made available on request.

## Acknowledgments

This research was supported by the National Natural Science Key Foundation of China (NSFC) (41930537) and Shanghai International Science and Technology Cooperation Fund Project (23230713800; 19230742700).

## Appendix A. Supplementary data

Supplementary data to this article can be found online at https://doi.org/10.1016/j.catena.2023.107601.

## References

Ai, B., Ma, C., Zhao, J., Zhang, R., 2020. The impact of rapid urban expansion on coastal mangroves: a case study in Guangdong Province China. Front. Earth Sci. 14 (1), 37–49.

Alizad, K., et al., 2018. Dynamic responses and implications to coastal wetlands and the surrounding regions under sea level rise. PLoS One 13 (10), e0205176.

Anthony, E.J., Besset, M., Dussouillez, P., Goichot, M., Loisel, H., 2019. Overview of the Monsoon-influenced Ayeyarwady River delta, and delta shoreline mobility in response to changing fluvial sediment supply. Mar. Geol. 417, 106038.

Baloloy, A., Blanco, A.C., Ana, R.R.C.S., Nadaoka, K., 2020. Development and application of a new mangrove vegetation index (MVI) for rapid and accurate mangrove mapping. ISPRS J. Photogramm. Remote Sens. 166, 95–117.

Besset, M., Anthony, E.J., Dussouillez, P., Goichot, M., 2017. The impact of Cyclone Nargis on the Ayeyarwady (Irrawaddy) River delta shoreline and nearshore zone (Myanmar): Towards degraded delta resilience? C. R. Geosci. 349 (6), 238–247.

Bhowmik, A.K., Padmanaban, R., Cabral, P., Romeiras, M.M., 2022. Global Mangrove Deforestation and Its Interacting Social-Ecological Drivers: A Systematic Review and Synthesis. Sustainability 14 (8), 4433.

Brakenridge, G.R., et al., 2017. Design with nature: Causation and avoidance of catastrophic flooding, Myanmar. Earth Sci. Rev. 165, 81–109.
Breiman, L., 2001. Random Forests. Mach. Learn. 45, 5–32.
Bryan-Brown, D., et al., 2020. Global trends in mangrove forest fragmentation. Sci. Rep. 10, 7117.
Bunting, P., et al., 2022. Global Mangrove Extent Change 1996–2020: Global Mangrove Watch Version 3.0. Remote. Sens. 14, 3657.
Burma. Ministry of Forestry and Kokusai Kyōryoku Jigyōdan, 2005. The study on integrated mangrove management through community participation in the Ayeyawady Delta in the Union of Myanmar: final report. Nippon Koei Co., Ltd, Tokyo.
Carugati, L., et al., 2018. Impact of mangrove forests degradation on biodiversity and ecosystem functioning. Sci. Rep. 8, 13298.
Chandrasekar, K., Sai, M.V.R.S., Roy, P.S., Dwevedi, R., 2010. Land Surface Water Index (LSWI) response to rainfall and NDVI using the MODIS Vegetation Index product. Int. J. Remote Sens. 31, 3987–4005.
Chang, D., et al., 2022. Vegetation changes in Yellow River Delta wetlands from 2018 to 2020 using PIE-Engine and short time series Sentinel-2 images. Frontiers in Marine. Science 9.
Clough, B.F., 1992. Primary Productivity and Growth of Mangrove Forests. In: A. I. Robertson, D.M.A. (A. I. Robertson, D.M.A.)˚(A. I. Robertson, D.M.A.s)|,*Tropical mangrove ecosystems. Coastal and Estuarine Studies. American Geophysical Union (AGU), Washington DC,. 225-249.
Conchedda, G., Durieux, L., Mayaux, P., 2008. An object-based method for mapping and change analysis in mangrove ecosystems. ISPRS J. Photogramm. Remote Sens. 63, 578–589.
Dahdouh-Guebas, F., et al., 2022. Cross-cutting research themes for future mangrove forest research. Nat. Plants 8 (10), 1131–1135.
Danielsen, F., et al., 2005. The Asian Tsunami: A Protective Role for Coastal Vegetation. Science 310, 643.
Duarte, C.M., Losada, I.J., Hendriks, I.E., Mazarrasa, I., Marbà, N., 2013. The role of coastal plant communities for climate change mitigation and adaptation. Nat. Clim. Chang. 3, 961–968.
Duke, N.C., et al., 2007. A World Without Mangroves? Science 317, 41–42.
Edmonds, D.A., et al., 2023. Land loss due to human-altered sediment budget in the Mississippi River Delta. Nat. Sustainability 6 (6), 644–651.
Ellison, A.M., Felson, A.J., Friess, D.A., 2020. Mangrove Rehabilitation and Restoration as Experimental Adaptive Management. Front. Mar. Sci. 7, 327.
Estoque, R.C., et al., 2018. Assessing environmental impacts and change in Myanmar's mangrove ecosystem service value due to deforestation (2000–2014). Glob. Chang. Biol. 24, 5391–5410.
Fanous, M., Eden, J.M., Remesan, R., Daneshkhah, A., 2023. Challenges and prospects of climate change impact assessment on mangrove environments through mathematical models. Environ Model Softw. 162, 105658.
Farr, T.G., et al., 2000. The Shuttle Radar Topography Mission. Rev. Geophys. 45 (2), RG2004.
Filipski, M. and Belton, B., 2017. Rural Economic Spillovers from Fish Farming and Agriculture in the Ayeyarwady Delta.: 7.
Friess, D.A., et al., 2019. The State of the World's Mangrove Forests: Past, Present, and Future. Annu. Rev. Env. Resour. 44, 89–115.
Fritz, H.M., Blount, C.D., Thwin, S., Thu, M.K., Chan, N., 2009. Cyclone Nargis storm surge in Myanmar. Nat. Geosci. 2 (7), 448–449.
Furuichi, T., Win, Z.A., Wasson, R.J., 2009. Discharge and suspended sediment transport in the Ayeyarwady River, Myanmar: centennial and decadal changes. Hydrol. Process. 23 (11), 1631–1641.
Gilman, E.L., Ellison, J.C., Coleman, R., 2007. Assessment of Mangrove Response to Projected Relative Sea-Level Rise And Recent Historical Reconstruction of Shoreline Position. Environ. Monit. Assess. 124, 105–130.
Giosan, L., et al., 2017. Short communication: Massive erosion in monsoonal central India linked to late Holocene land cover degradation. Earth Surf. Dyn. 5 (4), 781–789.
Giri, C., et al., 2011. Status and distribution of mangrove forests of the world using earth observation satellite data. Glob. Ecol. Biogeogr. 20, 154–159.
Giri, C.P., 2016. Observation and Monitoring of Mangrove Forests Using Remote Sensing: Opportunities and Challenges. Remote. Sens. 8, 783.
Gitau, P.N., Duvail, S.E.P., Verschuren, D., 2023. Evaluating the combined impacts of hydrological change, coastal dynamics and human activity on mangrove cover and health in the Tana River delta, Kenya. Regional Studies in Marine Science 61, 102898.
Glover, H.E., et al., 2022. Pathways for sediment transport and retention in a vegetated, mid-channel island: Connecting sediment dynamics to morphology in Meinmahla Island, Ayeyarwady Delta. Myanmar. Sedimentology 70 (1), 214–234.
Goldberg, L., Lagomasino, D., Thomas, N.M., Fatoyinbo, T.E., 2020. Global declines in human-driven mangrove loss. Glob. Chang. Biol. 26, 5844–5855.
Guo, Y., Liao, J., Shen, G., 2021. Mapping Large-Scale Mangroves along the Maritime Silk Road from 1990 to 2015 Using a Novel Deep Learning Model and Landsat Data. Remote. Sens. 13, 245.
Habibullah, I., Sanjaya, H., Putra, I.N.G., 2023. Utilization of the Indices to Detect and Monitor the Landcover Changes of Mangroves. IOP Conference Series: Earth and Environmental Science 1127 (1), 012033.
Hagger, V., et al., 2022. Drivers of global mangrove loss and gain in social-ecological systems. Nat. Commun. 13, 6373.
Hamilton, S.E., Casey, D., 2014. Creation of a high spatio-temporal resolution global database of continuous mangrove forest cover for the 21st century (CGMFC-21). Glob. Ecol. Biogeogr. 25, 729–738.
Heale, R., Twycross, A., 2015. Validity and reliability in quantitative studies. Evid. Based Nurs. 18 (3), 66–67.
Hedley, P.J., Bird, M.I., Robinson, R.A.J., 2010. Evolution of the Irrawaddy delta region since 1850. Geogr. J. 176 (2), 138–149.
Himmelstoss, E.A., Henderson, R.E., Kratzmann, M.G. and Farris, A.S., 2021. Digital Shoreline Analysis System (DSAS) version 5.1 user guide.: 51-52.
Hu, Z., et al., 2022. Wave Breaking Induced by Opposing Currents in Submerged Vegetation Canopies. Water Resour. Res. 58 (4), e2021WR031121.
Huang, Z., Dai, Z., Li, S., Huang, H., Feng, B., 2021. Erosion and accretion of a meso-macro-tidal beach profile - A case from the Yintan Beach of Beihai. Mar. Geol. Quat. Geol. 41 (4), 36–47. In Chinese with English abstract.
Huete, A.R., et al., 2002. Overview of the radiometric and biophysical performance of the MODIS vegetation indices. Remote Sens. Environ. 83, 195–213.
Ibharim, N.A.N., Mustapha, M.A., Lihan, T., Mazlan, A.G., 2015. Mapping mangrove changes in the Matang Mangrove Forest using multi temporal satellite imageries. Ocean Coast. Manag. 114, 64–76.
IPCC, 2022. Climate Change 2022: Impacts, Adaptation and Vulnerability. Contribution of Working Group II to the Sixth Assessment Report of the Intergovernmental Panel on Climate Change. Cambridge University Press, Cambridge, UK and New York, NY, USA, 3056.
IFC, 2019. Baseline Assessment Report Geomorphic and Sediment Transport - Strategic Environmental Assessment of the Hydropower Sector in Myanmar. In: No, 134197. The World Bank Group. 18.
Jayanthi, M., et al., 2023. Are the Sundarbans, the World's largest mangroves region under threat?—An ecosystem-based geospatial approach to assess changes past, present, and future in relation to natural and human-induced factors. Land Degrad. Dev. 34 (1), 125–141.
Jia, M., et al., 2014. Mapping China's mangroves based on an object-oriented classification of Landsat imagery. Wetlands 34, 277–283.
Jia, M., et al., 2023. Mapping global distribution of mangrove forests at 10-m resolution. Science Bulletin.
Kimeli, A., et al., 2022. Surface elevation changes in an estuarine mangrove forest in Vanga, Kenya: Implications for management and mitigation of sea-level rise. Frontiers in Marine. Science 932963.
Krauss, K.W., et al., 2014. How mangrove forests adjust to rising sea level. New Phytol. 202 (1), 19–34.
Leal, M. and Spalding, M.D., 2022. The state of the world's mangroves 2022, Global Mangrove Alliance.
Liang, S., et al., 2022. Mapping mangrove sustainability in the face of sea level rise and land use: A case study on Leizhou Peninsula. China. Journal of environmental management 325 (Pt B), 116554.
Liao, J., Zhen, J., Zhang, L., Metternicht, G.I., 2019. Understanding Dynamics of Mangrove Forest on Protected Areas of Hainan Island, China: 30 Years of Evidence from Remote Sensing. Sustainability 11 (19), 5356.
Long, C., et al., 2022. Dynamic changes in mangroves of the largest delta in northern Beibu Gulf, China: Reasons and causes. For. Ecol. Manage. 504 (15), 119855.
Long, C., Dai, Z., Zhou, X., Mei, X., Van, C.M., 2021. Mapping mangrove forests in the Red River Delta. Vietnam. Forest Ecology and Management 483, 118910.
Lovelock, C.E., et al., 2015. The vulnerability of Indo-Pacific mangrove forests to sea-level rise. Nature 526, 559–563.
Lovelock, C.E., Reef, R., Masqué, P., 2021. Vulnerability of an arid zone coastal wetland landscape to sea level rise and intense storms. Limnol. Oceanogr. 66 (11), 3976–3989.
Mafi-Gholami, D., Zenner, E.K., Jaafari, A., 2020. Mangrove regional feedback to sea level rise and drought intensity at the end of the 21st century. Ecol. Ind. 110, 105972.
Mahdavi, S., et al., 2018. Remote sensing for wetland classification: a comprehensive review. GIScience & Remote Sensing 55 (5), 623–658.
Mai Van, C., Ngo, A., Mai, T., Dao, H.T., 2021. Bamboo Fences as a Nature-Based Measure for Coastal Wetland Protection in Vietnam. In: Frontiers in Marine Science, p. 8.
McGarigal, K. and Marks, B.J., 1995. FRAGSTATS: spatial pattern analysis program for quantifying landscape structure.: 122.
Mokievsky, V.O., Son, T., Dobrynin, D.V., 2020. The Dynamics of Mangroves in the Mekong Delta (Vietnam): From Degradation to Restoration. Dokl. Earth Sci. 494 (1), 745–747.
Murillo-Sandoval, P.J., Fatoyinbo, L. and Simard, M., 2022. Mangroves Cover Change Trajectories 1984-2020: The Gradual Decrease of Mangroves in Colombia, Frontiers in Marine Science. 892946.
Nanda, A.M., 2014. The Effects of Global Warming in Myanmar since 2000. Dagon University Research Journal 6, 91–96.
Ono, K., 2007. Locally appropriate management of mangrove ecosystem: a case study in the Ayeyarwady delta. Yokohama National University, Yokohama, Myanmar.
Oo, N.W., 2002. Present state and problems of mangrove management in Myanmar. Trees 16, 218–223.
Pike, R.J., Rozema, W.J., 1975. Spectral Analysis of Landforms. Ann. Assoc. Am. Geogr. 65 (4), 499–516.
Poortinga, A., et al., 2020. Predictive Analytics for Identifying Land Cover Change Hotspots in the Mekong Region. Remote. Sens. 12, 1472.
Prasad, P., Loveson, V.J., Chandra, P., Kotha, M., 2022. Evaluation and comparison of the earth observing sensors in land cover/land use studies using machine learning algorithms. Eco. Inform. 68, 101522.
Qu, S., Wang, L., Lin, A., Zhu, H., Yuan, M., 2018. What drives the vegetation restoration in Yangtze River basin, China: Climate change or anthropogenic factors? Ecol. Ind. 90, 438–450.

Raw, J.L., et al., 2022. Dispersal and coastal geomorphology limit potential for mangrove range expansion under climate change. J. Ecol. 111, 139–155.
Richards, D.R., Thompson, B.S., Wijedasa, L.S., 2020. Quantifying net loss of global mangrove carbon stocks from 20 years of land cover change. Nat. Commun. 11, 4260.
Salem, M.E., Mercer, D.E., 2012. The Economic Value of Mangroves: A Meta-Analysis. Sustainability 4, 359–383.
Sánchez-Núñez, D.A., Bernal, G., Mancera Pineda, J.E., 2019. The Relative Role of Mangroves on Wave Erosion Mitigation and Sediment Properties. Estuar. Coasts 42 (8), 2124–2138.
Scott, L.M. and Janikas, M.V., 2010. Spatial Statistics in ArcGIS. In: Fischer, M.M. and Getis, A. (Fischer, M.M. and Getis, A.)^(Fischer, M.M. and Getis, A.s)|,*Handbook of Applied Spatial Analysis: Software Tools, Methods and Applications. Springer, Berlin, Heidelberg,. 27–41.
Shi, T., et al., 2016. New spectral metrics for mangrove forest identification. Remote Sensing Letters 7, 885–894.
Spalding, M.D., McIvor, A.L., Tonneijck, F.H., Tol, S. and van Eijk, P., 2014. Mangroves for Coastal Defence: Guidelines for coastal managers & policy makers.: 42.
Spalding, M., Kainuma, M., Collins, L., 2010. World Atlas of Mangroves, 31. Earthscan, London, p. 336.
Swales, A., Reeve, G., Cahoon, D.R., Lovelock, C.E., 2019. Landscape Evolution of a Fluvial Sediment-Rich Avicennia marina Mangrove Forest: Insights from Seasonal and Inter-annual Surface-Elevation Dynamics. Ecosystems 1–24.
Tatsumi, K., Yamashiki, Y.A., Torres, M.A.O.N., Taipe, C.L.R., 2015. Crop classification of upland fields using Random forest of time-series Landsat 7 ETM+ data. Comput. Electron. Agric. 115, 171–179.
Teluguntla, P.G., et al., 2018. A 30-m landsat-derived cropland extent product of Australia and China using random forest machine learning algorithm on Google Earth Engine cloud computing platform. ISPRS J. Photogramm. Remote Sens. 144, 325–340.
Thomas, N.M., et al., 2017. Distribution and drivers of global mangrove forest change, 1996–2010. PLoS One 12 (6), e0179302.
Thu, P.M., Populus, J., 2007. Status and changes of mangrove forest in Mekong Delta: Case study in Tra Vinh. Vietnam. Estuarine Coast. Shelf Sci. 71, 98–109.
Tinh, P.H., et al., 2022. Distribution and drivers of Vietnam mangrove deforestation from 1995 to 2019. Mitig. Adapt. Strat. Glob. Chang. 27 (4), 29.
Tran Thi, V., Tien Thi Xuan, A., Phan Nguyen, H., Dahdouh-Guebas, F., Koedam, N., 2014. Application of remote sensing and GIS for detection of long-term mangrove shoreline changes in Mui Ca Mau, Vietnam. Biogeosciences 11 (14), 3781–3795.
Tucker, C.J., 1979. Red and photographic infrared linear combinations for monitoring vegetation. Remote Sens. Environ. 8, 127–150.
Valderrama-Landeros, L.H., et al., 2020. Regional Distribution and Change Dynamics of Mangroves in Mexico between 1970/80 and 2015. Wetlands 40, 1295–1305.
Wang, F., et al., 2014. Island instantaneous coastline extraction based on the characteristics of regional statistics of multispectral remote sensing image. Acta Oceanol. Sin. 16 (1), 25–37. In Chinese with English abstract.
Waryszak, P., Gavoille, A., Whitt, A.A., Kelvin, J., Macreadie, P.I., 2021. Combining gray and green infrastructure to improve coastal resilience: lessons learnt from hybrid flood defenses. Coast. Eng. J. 63 (3), 335–350.
Win, S., Towprayoon, S., Chidthisong, A., 2020. Mangrove status, its ecosystem, and climate change in Myanmar: A study in Ayeyarwaddy Delta Coastal Zone. IOP Conference Series: Earth and Environmental Science 496 (1), 012007.
Woodroffe, C.D., et al., 2016. Mangrove Sedimentation and Response to Relative Sea-Level Rise. Ann. Rev. Mar. Sci. 8, 243–266.
Worthington, T.A., et al., 2020. Harnessing Big Data to Support the Conservation and Rehabilitation of Mangrove Forests Globally. One Earth 2 (5), 429–443.
Wu, J., 2000. Landscape ecology - Pattern, process and hierarchy. Higher Education press, Beijing, 108-111. (In Chinese with English abstract).
Xiao, X., et al., 2002. Observation of flooding and rice transplanting of paddy rice fields at the site to landscape scales in China using VEGETATION sensor data. Int. J. Remote Sens. 23, 3009–3022.
Xiao, X., et al., 2004. Modeling gross primary production of temperate deciduous broadleaf forest using satellite images and climate data. Remote Sens. Environ. 91, 256–270.
Xie, D., Schwarz, C., Kleinhans, M.G., Zhou, Z., van Maanen, B., 2022. Implications of Coastal Conditions and Sea-Level Rise on Mangrove Vulnerability: A Bio-Morphodynamic Modeling Study. J. Geophys. Res. Earth Surf. 127 (3), e2021JF006301.
Xu, H., 2006. Modification of normalised difference water index (NDWI) to enhance open water features in remotely sensed imagery. Int. J. Remote Sens. 27, 3025–3033.
Zhang, S., 2008. Spatio-temporal dynamic changes of China's typical wetland landscape supported by 3S. Jilin University Press, Changchun, Jilin, pp. 273–294. In Chinese with English abstract.
Zhang, B., et al., 2022. Super-resolution reconstruction of a 3 arc-second global DEM dataset. Science Bulletin 67 (24), 2526–2530.
Zhang, Z., Ahmed, M.R., Zhang, Q., Li, Y., Li, Y., 2023. Monitoring of 35-Year Mangrove Wetland Change Dynamics and Agents in the Sundarbans Using Temporal Consistency Checking. Remote Sens. (Basel) 15, 625.
Zöckler, C., Delany, S. and Barber, J., 2013. Sustainable coastal zone management in Myanmar.